Micromachined Hot-Filament Ionization Pressure Sensor and Magnetometer

Kirt R. Williams* and Richard S. Muller
Berkeley Sensor & Actuator Center, 497 Cory Hall, U.C. Berkeley, Berkeley, CA 94720-1770, USA
*Present address: Lucas NovaSensor, 1055 Mission Court, Fremont, CA 94539, USA

SUMMARY

Two new micromachined sensors, an ionization pressure sensor (ion gauge) and magnetic-field sensor, were fabricated and tested. Both sensors employ electrons thermionically emitted from a hot tungsten filament for sensing and are built using the same fabrication process.

Keywords: thermionic, pressure, magnetic

DEVICE STRUCTURE

In these hot-filament vacuum devices, 500-μm-long tungsten bridges span a cavity etched into a silicon substrate to form free-standing filaments (Fig. 1). During operation, a sufficiently large current is passed through one or more filaments (cathodes) to heat them to incandescence and cause the thermionic emission of electrons. Depending on the arrangement and voltages applied to other filaments, these micro-emitting devices can be operated as thermionic diodes or triodes [1,2], or they can function as sensors.

The tungsten is isolated electrically and thermally from the silicon substrate by dielectric layers of silicon nitride and phosphosilicate glass (PSG). The substrate is heavily doped n-type silicon to make it electrically conductive in order to reduce electron-charge buildup on the cavity walls.

Stress-relief folds (Fig. 1a) are added to some of the freestanding filaments to allow thermal expansion at lower stress levels and to reduce breakage during processing. The 500 μm length refers to the electrical path length; the linear distance from anchor point to anchor point depends on the shape of the stress-relief folds.

In operation, the centers of the hot filaments are at approximately 2800 K and have a lifetime of about an hour of continuous operation. (This lifetime could be improved to several weeks with the use of a low-work-function coating, which would allow lower-temperature operation.) To avoid oxidation and rapid burnout of the hot filaments, and to allow for long electron mean-free-path lengths, the devices are operated in a pumped vacuum chamber.

FABRICATION

Fabrication begins with a (100)-oriented, n-type silicon wafer with the heaviest doping readily available. A 1 μm layer of PSG is low-pressure chemical-vapor deposited (LPCVD) from $SiH_4 + O_2 + PH_3$ and annealed in N_2 (done to avoid outgassing during subsequent high-temperature steps). This is followed by the LPCVD from $SiCl_2H_2 + NH_3$ of 0.5 μm silicon-rich (low-stress) silicon nitride to form the "field" area.

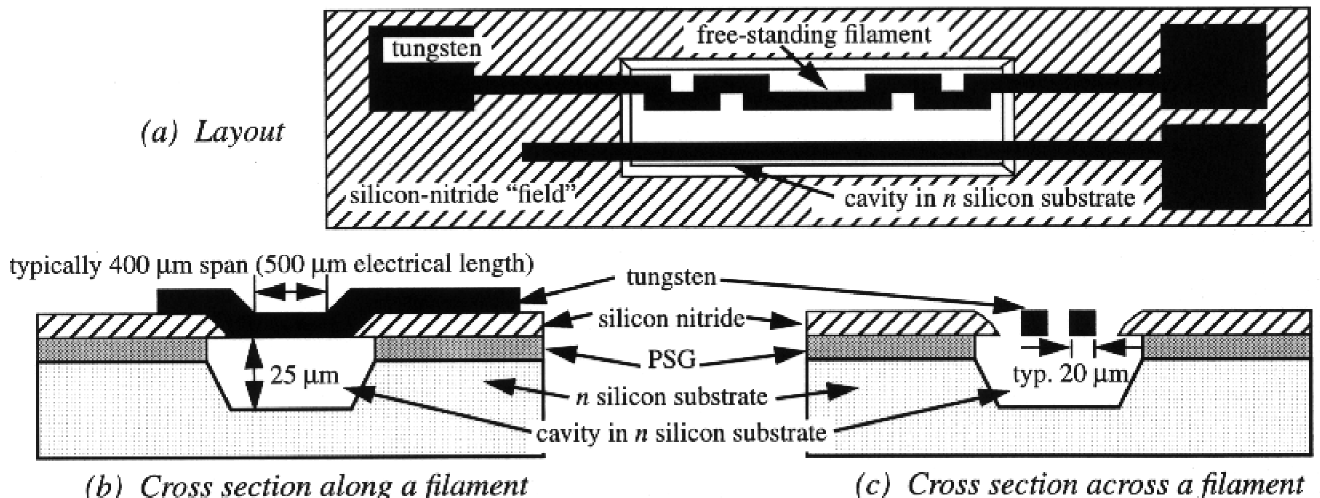

Figure 1: Hot-filament vacuum device structure

The area outside of the window in the field nitride, which will define the cavity, is masked with photoresist. 0.3 μm of the nitride in the window area is plasma-etched in SF_6, followed by unmasked wet etching in hot phosphoric acid through the remainder of the nitride. This is done to round off the nitride step and to ensure stopping at the silicon, which avoids later formation of tungsten stringers (Fig. 2).

Next, a thin adhesion layer of reactively sputtered titanium nitride (Ti in Ar + N_2) is deposited. Without breaking vacuum, 2.2 μm of low-residual-stress tungsten is sputtered. This is relatively thick for a tungsten film using IC-fabrication-type processing, and required the selection of an appropriate sputter-gas pressure to yield a low tensile stress about 200 MPa (Fig. 3) [3,2]. (Thick tungsten is desired so that the filaments have long lifetimes.) The tungsten is patterned with photoresist and reactive-ion-etched in SF_6 to define the filaments, interconnect, and pad areas.

Aluminum, 0.5 μm thick, is sputtered, patterned with photoresist, and wet etched to form bond pads. The photoresist mask is left on the pads for protection during the next step.

At this point the wafer is divided into chips with a dicing saw. This is done before release of the filaments because it was found that cleaving after release resulted in breakage of most of the filaments.

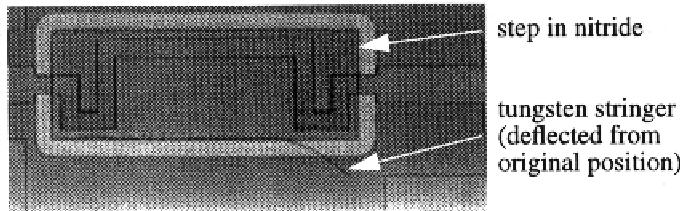

Figure 2: Tungsten stringers caused by vertical underlying silicon-nitride step

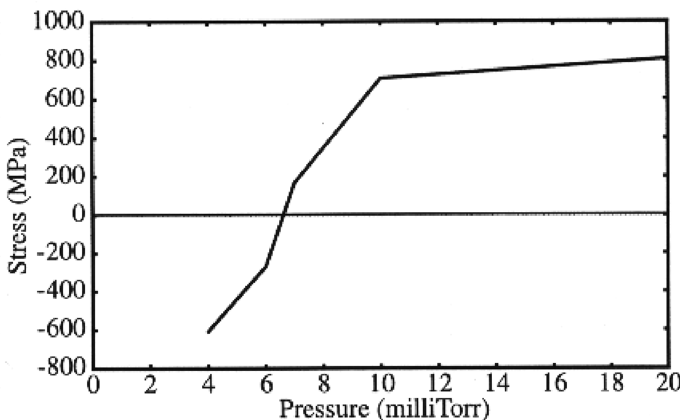

Figure 3: Tungsten stress vs. argon sputter pressure in CPA sputterer at 2.0 kW power

The PSG is removed from the cavity area during a timed etch in 5:1 buffered hydrofluoric acid (BHF). The etch also undercuts the tungsten filaments and the nitride field (the light-colored ring in Fig. 2).

Finally, a 25-μm-deep cavity (Fig. 1) is formed in the silicon substrate using a timed etch in hot potassium hydroxide. The tungsten filaments are not attacked appreciably in BHF or KOH [4]. The aluminum pads are unintentionally removed in the KOH; future processing could instead use silicon-doped tetramethylammonium hydroxide, which has been found not to attack aluminum [5].

IONIZATION PRESSURE SENSOR

In the ion gauge (Fig. 4), electrons emitted by the cathode are accelerated to, and collected by, the adjacent filaments, which are held at 100 V (Fig. 4b). Energetic electrons that collide with gas molecules generate positive ions which are collected by the next pair of filaments, biased at –40V. A grounded ring surrounds the device to shield it. A symmetrical device structure is used to double the ion and electron currents. Figure 4c shows a cross-sectional simulation of electron paths using an adapted version of the plasma simulator PDP2 [6].

Theoretically, the ion current I_i is proportional to the electron current I_e, the gas pressure p, the ionization rate α of the ambient gas, and the electron path length L

$$I_i = I_e p \alpha L \quad . \tag{1}$$

To remove the dependence of I_i on fluctuations in electron current, the output variable is typically normalized to I_i/I_e rather than simply I_i [7,8]. The sensitivity S is defined as the ratio of (I_i/I_e) to p

$$S = (I_i/I_e)/p \quad . \tag{2}$$

From Eq. 1, S also equals αL. However, because in this sensor some electrons generate ions but are not collected to contribute to I_e (Fig. 4c), we add a factor f (> 1) to increase S, giving

$$S = \alpha L f \quad . \tag{3}$$

Using $\alpha = 7.8\ \text{cm}^{-1}\ \text{Torr}^{-1}$ for air [7] and from the simulation estimating L and f to be 150-250 μm and 1.5-2.5, respectively, we estimate S to be in the range 0.18-0.49 Torr^{-1}. (In practice, the average electron-path length in ion gauges is difficult to predict

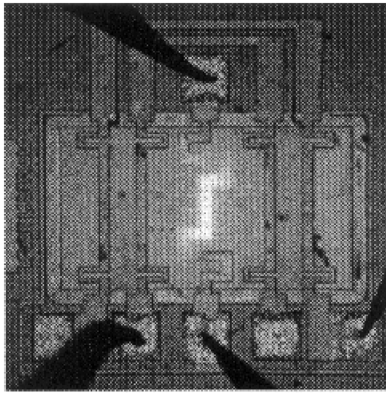

(a) Photomicrograph during operation

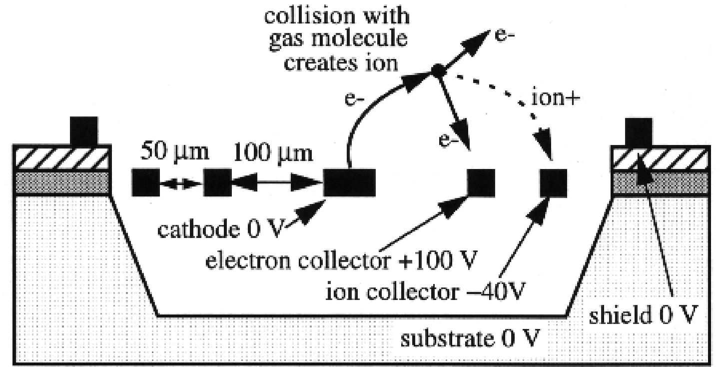

(b) Cross section/operation

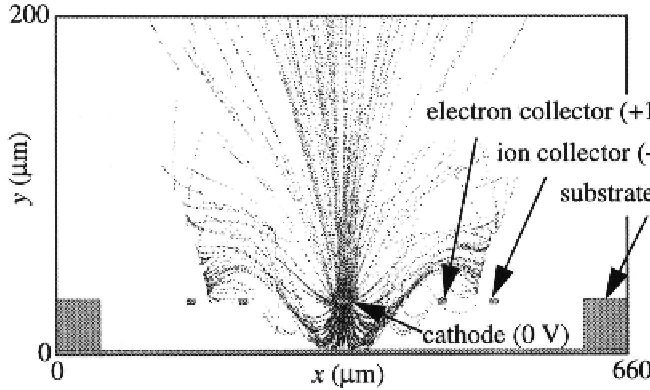

(c) Cross-sectional simulation of electron paths using PDP2

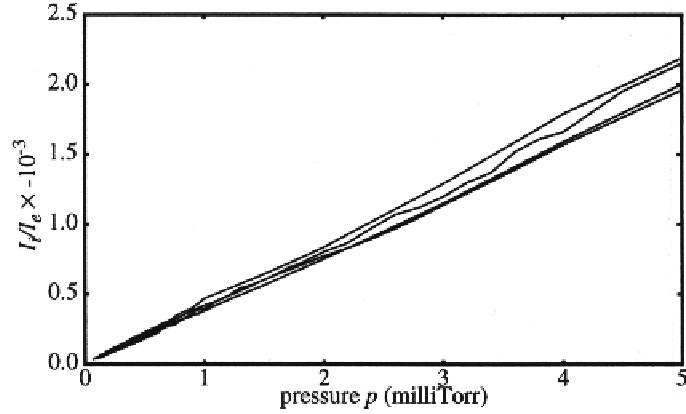

(d) I_i/I_e *vs. pressure*

Figure 4: Micromachined ionization pressure sensor

due to the spiral paths [7].)

In the operation of several devices over a pressure range of 7×10^{-5} to 1.3×10^{-2} Torr (varied by turning off the pump in our vacuum system and allowing air to leak in), the measured response is linear and fairly reproducible. The average sensitivity is 0.42 Torr^{-1} (Fig. 4d), within our estimated range.

This ion gauge occupies a volume that is orders of magnitude smaller than its conventionally sized counterpart, making the gauge suitable for pressure measurements in, for example, a microchip package.

MAGNETIC-FIELD SENSOR

In the magnetic-field sensor (Fig. 5), a symmetrical pair of hot-filament cathodes emits electrons. These filaments are designed so that their hottest regions are on either side of and close to the center line of the device (Fig. 5a), which concentrates thermionically emitted electrons along this center line. A potential of +100 V is applied to the symmetrical pair of anodes at the opposite end of the device (Fig. 5b). The electrons form a "beam" (of width y_{beam}, roughly equal to the width of the pair of cathodes) as they flow from the cathodes to the anodes. This is an improvement over a previous field-emission magnetic-field sensor that did not have a narrowly defined beam [9].

In the absence of a magnetic field, the anode currents are equal. With a small vertical magnetic field B_z applied, however, the Lorentz force causes the beam to shift by Δy to one side (Fig. 5c) (a large field would result in cycloid motion). The shift is given by

$$\Delta y = \left(\frac{2q}{mV_A}\right)^{1/2} \frac{x_0^2}{3} B_z \qquad (4)$$

where q and m are the electron charge and mass, V_A is the anode voltage, and x_0 is the cathode-to-anode spacing [2].

The beam shift results in an increase in anode current ΔI_A in one anode and a corresponding decrease in the other. The fractional current change is

$$\frac{\Delta I_A}{I_{A,\,tot}} = \frac{I_{A1} - I_{A2}}{I_{A1} + I_{A2}} = \frac{2\Delta y}{y_{beam}} \qquad (5)$$

where I_{A1} and I_{A2} are the anode currents and $I_{A,tot}$ is

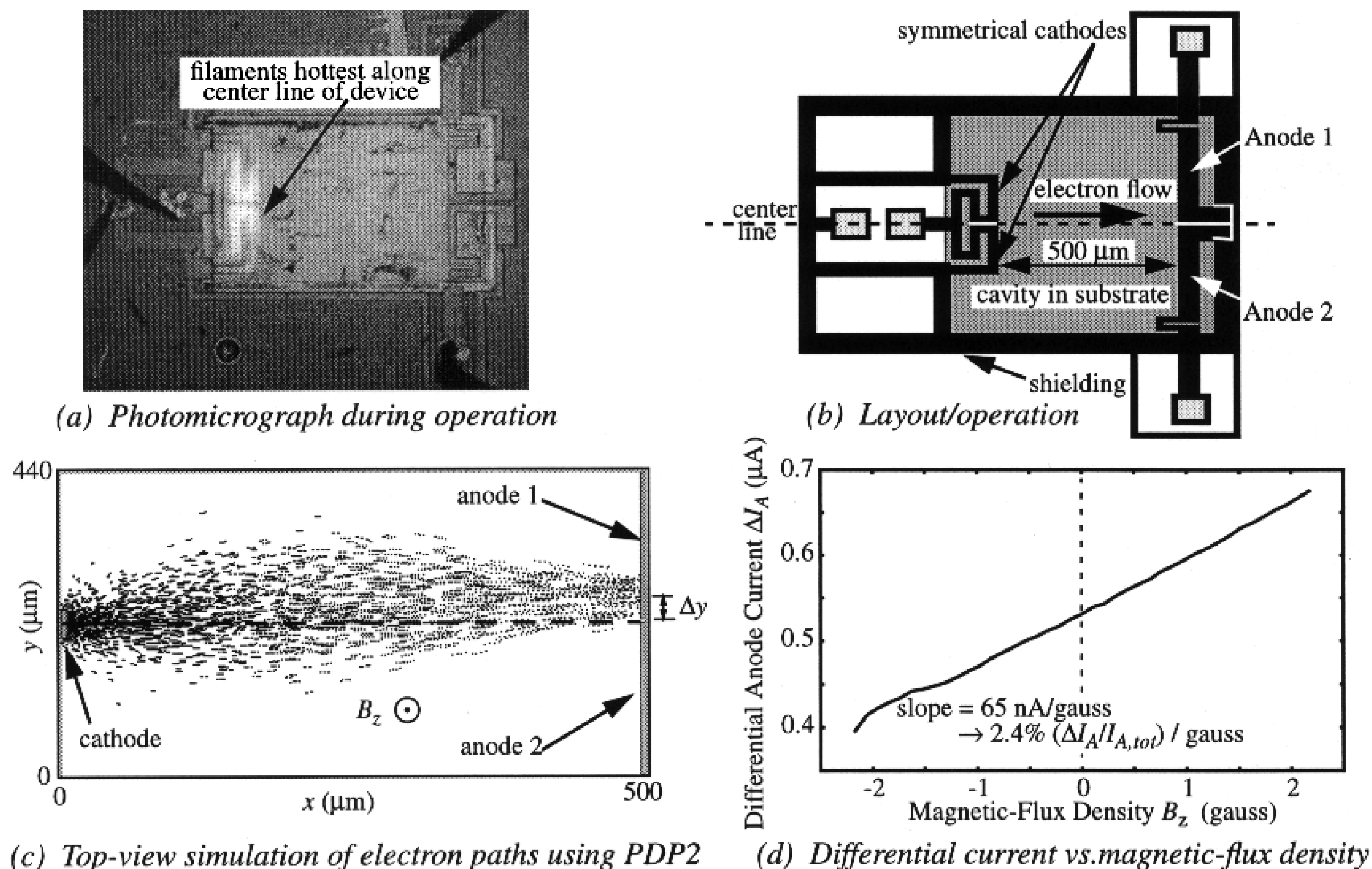

(a) Photomicrograph during operation *(b) Layout/operation*

(c) Top-view simulation of electron paths using PDP2 *(d) Differential current vs.magnetic-flux density*

Figure 5: Micromachined magnetic-field sensor

their sum.

For y_{beam} = 40 µm, x_0 = 500 µm, and V_A = 100 V, we estimate the slope of the fractional current change *vs.* magnetic-flux density to be 2.5%/gauss. Using a Helmholtz coil to apply a magnetic field, we measured a response of 2.4%/gauss (Fig. 5d). This sensor has roughly the same sensitivity as a comparably sized magnetotransistor [10].

It is critical in the magnetic-field-sensor design that two symmetrical cathode filaments with equal and opposite currents are used. This results in the magnetic fields generated by the cathode-heating currents cancelling each other out. The offset in Fig. 5d could be due to imperfect cancellation, as well as to stray dc magnetic or electric fields in the vicinity.

ACKNOWLEDGMENTS

This work was funded by the Berkeley Sensor & Actuator Center. Fabrication was done in the Berkeley Microfabrication Laboratory. We thank UCB Plasma Theory and Simulation Group for PDP2.

REFERENCES

[1] K. R. Williams and R. S. Muller, "IC-processed hot-filament vacuum microdevices," *Tech. Dig. IEDM*, 1992, pp. 387-390.

[2] Kirt R. Williams, *Micromachined Hot-Filament Vacuum Devices*, Ph.D. diss., EECS Dept. U.C. Berkeley, 1997.

[3] D.W. Hoffman and John A. Thorton, "The compressive stress transition in Al, V, Zr, Nb, and W metal films sputtered at low working pressures," *Thin Solid Films*, vol. 45, pp. 387-396, 1977.

[4] K. R. Williams and R. S. Muller, "Etch rates for micromachining processing," *Journal of Microelectromechanical Systems*, vol. 5, no. 4, pp. 256-269, Dec. 1996.

[5] U. Schnakenberg, W. Benecke, and P. Lange, "TMAHW etchants for silicon micromachining," *Tech. Dig. Transducers '91*, 1989, pp. 815-818.

[6] V. Vahedi, and G. DiPeso, "Simultaneous Potential and Circuit Solution for Two-Dimensional Bounded Plasma Simulation Codes," *Journal of Computational Physics*, 1997.

[7] Norman Robinson, *The Physical Principles of Ultra-High Vacuum*, Chapman & Hall, London, 1968, Ch. 1.

[8] F. M. Penning, "High-vacuum gauges," *Phillips Tech. Rev.*, vol. 2, 1937, p. 205.

[9] Y. Sugiyama, J. Itoh, and S. Kanemaru, "Vacuum magnetic sensor with comb-shaped field emitter arrays," *Tech. Dig. Transducers '93*, pp. 884-887.

[10] J. E. Lenz, "A review of magnetic sensors," Proc. IEEE, vol. 78, no. 6, June 1990, pp. 973-989.